Supporting Information

Chen et al. 10.1073/pnas.1405969111

SI Appendix

Soliton in the Flipper Phase

In this section, we derive the continuum ϕ^4 theory that describes the domain wall (soliton) solution in the flipper phase of motion. The discrete Lagrangian for the one-dimensional mechanical analog of the Su–Schrieffer–Heeger (SSH) chain is

$$L=\sum_n \frac{1}{2}I\left(\frac{d\theta_n}{dt}\right)^2-\frac{1}{2}k_e\left(l_{n,n+1}-\bar{l}\right)^2, \qquad [S1]$$

where, $I=M_r{}^2$ is the moment of inertia of the rod–mass system, θ_n is the angular position of the nth rod measured with respect to the positive direction of the y axis, k_e is the bare spring constant between neighboring rods with rest length $\bar{l}$, and $l_{n,n+1}$ is the instantaneous length of the spring connecting rods n and $n+1$.

We make the working assumption that throughout the course of the motion, the lengths of the springs do not change appreciably from their rest length; that is, we consider the springs to be almost rigid. Thus, a more tractable continuum limit follows by expressing the potential energy in Eq. **S1** as

$$\frac{1}{2}k_e\left(l_{n,n+1}-\bar{l}\right)^2=\frac{1}{2}\frac{k_e}{\left(l_{n,n+1}+\bar{l}\right)^2}\left(l_{n,n+1}+\bar{l}\right)^2\left(l_{n,n+1}-\bar{l}\right)^2 \qquad [S2]$$

$$\approx\frac{\kappa}{2}\left(l_{n,n+1}^2-\bar{l}^2\right)^2, \qquad [S3]$$

where in the last step we have assumed that $(l_{n,n+1}+\bar{l})^2\approx 4\bar{l}^2$ and so the potential energy is approximately unchanged if we define a new spring constant $\kappa=k_e/4\bar{l}^2$. Next, by expressing $l_{n,n+1}$ in terms of the angles θ_n, θ_{n+1} and the geometrical parameters r, a, we find the potential part of the Lagrangian to be

$$V_{n,n+1}[\theta_n,\theta_{n+1}]=2\kappa r^4\left[\cos(\theta_n+\theta_{n+1})-\cos(2\bar{\theta})+\frac{a}{r}(\sin\theta_n-\sin\theta_{n+1})\right]^2. \qquad [S4]$$

Next, we take the continuum limit, assuming $a\to dx$, $\theta_n\to\theta(x)-(a/2)(d\theta/dx)$, $\theta_{n+1}\to\pi-\theta(x)-(a/2)(d\theta/dx)$ (taking a Taylor series centered at $x=n+1/2$), to obtain the potential energy density as a perfect square

$$V[u(x)]=\frac{K}{2}\left[\left(\bar{u}^2-u(x)^2\right)+\frac{a^2}{2}\frac{du(x)}{dx}\right]^2, \qquad [S5]$$

where we denote the projection of the rods along the $\hat{x}$ axis by $u(x)=r\sin\theta(x)$ and define the constants $\bar{u}=r\sin\bar{\theta}$ and $K=16\kappa=4k_e/\bar{l}^2$.

Thus, in the continuum limit and expressed in terms of the field $u(x,t)$, Eq. **S1** assumes the form

$$\mathcal{L}=\int dx\left\{\frac{1}{2}\frac{Mr^2}{r^2-u^2}\left(\frac{\partial u}{\partial t}\right)^2-\frac{1}{2}K\frac{a^4}{4}\left(\frac{\partial u}{\partial x}\right)^2-\frac{1}{2}K\left(\bar{u}^2-u^2\right)^2-\frac{1}{2}K\frac{a^2}{2}\left(\bar{u}^2-u^2\right)\frac{\partial u}{\partial x}\right\}. \qquad [S6]$$

Eq. **S6** differs from the ordinary ϕ^4 theory due to the presence of the last term (linear in $\partial u/\partial x$) and because of the nonlinear kinetic term. As explained in the main text, the last term is related to the topological charge of the soliton that ensures that the static kink costs zero potential energy and does not contribute to the equation of motion. Moreover, by expanding the nonlinear kinetic term to order u^2/r^2 (valid in the limit of small $\bar{\theta}$), we obtain from Eq. **S6** the ordinary ϕ^4 theory, whose soliton solution is

$$u=\bar{u}\tanh\left[\frac{x-x_0-vt}{(a^2/2\bar{u})\sqrt{1-v^2/c^2}}\right], \qquad [S7]$$

where v is the speed at which the kink propagates and the effective "speed of light" is $c=(a^2/\bar{l})\sqrt{k_e/M}$. This coincides with Eq. **11** in the main text.

Soliton in the Spinner Phase

As discussed in the main text, to obtain the soliton solution in the spinner phase, we define the continuum field as the slowly varying angular field of odd or even sites. In the following, we discuss an approximate method for describing odd (even) fields, whose soliton solutions can be described by the sine-Gordon theory. Consider Eq. **S1** (writing three terms), assuming n is an odd site, for instance, and with the working assumption that $(l_{n,n+1}+\bar{l})^2\approx 4\bar{l}^2$,

$$L=\sum_n \frac{1}{2}I\dot{\theta}_n^2+\frac{1}{2}I\dot{\theta}_{n+1}^2+\frac{1}{2}I\dot{\theta}_{n+2}^2-\frac{k_e}{8\bar{l}^2}\left(l_{n,n+1}^2-\bar{l}^2\right)^2-\frac{k_e}{8\bar{l}^2}\left(l_{n+1,n+2}^2-\bar{l}^2\right)^2-\frac{k_e}{8\bar{l}^2}\left(l_{n+2,n+3}^2-\bar{l}^2\right)^2, \qquad [S8]$$

where dots denote derivative with respect to time.

To combine odd (even) sites, consider combining half of the potential energies at a time, so that both odd and even sites get their share from the same Lagrangian. To do this, we express the potential energy as a sum of terms of the following form:

$$V=\frac{k_e}{16\bar{l}^2}\sum_n\left[\left(l_{n,n+1}^2-\bar{l}^2\right)^2+\left(l_{n+1,n+2}^2-\bar{l}^2\right)^2\right]+\sum_n\left[\left(l_{n+1,n+2}^2-\bar{l}^2\right)^2+\left(l_{n+2,n+3}^2-\bar{l}^2\right)^2\right]. \qquad [S9]$$

For instance, the first square bracket can now be used to integrate out an even site and the second one to integrate out an odd site. Consider the first square bracket reexpressed as

$$\left[\left(l_{n,n+1}^2-\bar{l}^2\right)^2+\left(l_{n+1,n+2}^2-\bar{l}^2\right)^2\right]=\frac{1}{2}\left[\left(l_{n,n+1}^2+l_{n+1,n+2}^2-2\bar{l}^2\right)^2+\left(l_{n,n+1}^2-l_{n+1,n+2}^2\right)^2\right]. \qquad [S10]$$

Assuming that the average of $l_{n,n+1}^2+l_{n+1,n+2}^2=2\bar{l}^2$, the first term in the above equation can be approximated to 0. We are thus left with

$$\left[\left(l_{n,n+1}^2-\bar{l}^2\right)^2+\left(l_{n+1,n+2}^2-\bar{l}^2\right)^2\right]=\frac{1}{2}\left[\left(l_{n,n+1}^2-l_{n+1,n+2}^2\right)^2\right]. \qquad [S11]$$

After substituting the lengths by angles and r, a, we obtain

$$l_{n,n+1}^2 - l_{n+1,n+2}^2 = 2r^2\left[\cos(\theta_n - \theta_{n+1}) - \cos(\theta_{n+1} - \theta_{n+2}) + \frac{a}{r}\left[\sin(\theta_n) + \sin(\theta_{n+2}) - 2\sin(\theta_{n+1})\right]\right]. \quad \text{[S12]}$$

As discussed in the main text, we take the continuum limit by defining the field $\theta_n \to \theta(x)$ and $\theta_{n+2} \to \theta(x+2a) = \theta + 2a(d\theta/dx)$ and then retaining terms to leading order in a. We "integrate out" θ_{n+1} (the degree of freedom representing the middle rod) by using the constraint equation $l_{n,n+1}^2 = \bar{l}^2$. Expressing this second constraint equation in terms of the angles $\{\bar{\theta}, \theta_n, \theta_{n+1}\}$, we find (in the limit $a \ll r$) that $\theta_{n+1} \approx \theta_n + \pi - 2\bar{\theta}$. We thus obtain the following potential energy contribution from the odd sites:

$$V_o = \frac{k_e r^4 a^2 \sin^2(2\bar{\theta})}{2\bar{l}^2}\left[\frac{d\theta}{dx} - \frac{a}{r\sin\bar{\theta}}\sin(\theta - \bar{\theta})\right]^2. \quad \text{[S13]}$$

We therefore identify an effective spring constant $K^{\text{eff}} = k_e r^4 a^2 \sin^2(2\bar{\theta})/\bar{l}^2$. Similarly, combining half of the kinetic energies from the odd sites $(1/4)Mr^2\dot{\theta}_n^2 + (1/4)Mr^2\dot{\theta}_{n+2}^2$, we obtain $(1/2)Mr^2\dot{\theta}^2$. Therefore, the moment of inertia is $I = Mr^2$.

With this procedure, we have therefore expressed the Lagrangian as a sine-Gordon Lagrangian for the odd (even) sites, whose continuum limit for the odd (o) sites reads

$$\mathcal{L}_o = \int dx\left\{\frac{1}{2}I\dot{\theta}_o^2 - \frac{1}{2}K^{\text{eff}}\left[\theta_o' - \frac{a}{r\sin\bar{\theta}}\sin(\theta_o - \bar{\theta})\right]^2\right\}, \quad \text{[S14]}$$

while for the even (e) sites, we find

$$\mathcal{L}_e = \int dx\left\{\frac{1}{2}I\dot{\theta}_e^2 - \frac{1}{2}K^{\text{eff}}\left[\theta_e' + \frac{a}{r\sin\bar{\theta}}\sin(\theta_e + \bar{\theta})\right]^2\right\}, \quad \text{[S15]}$$

where primes denote derivative with respect to space x. Upon using the Euler–Lagrange equations, we obtain the respective soliton solutions

$$\cos(\theta \pm \bar{\theta}) = \pm\tanh\left(\frac{x - vt}{r\sin(\bar{\theta})\sqrt{1 - v^2/c^2}}\right), \quad \text{[S16]}$$

where, $\pm$ corresponds to soliton solutions for the even (odd) sites, respectively (which are of course constrained so that $\theta_e = \theta_o + \pi - 2\bar{\theta}$), and where c, the speed of sound in the spinner phase $r \gg a$, is

$$c = \sqrt{\frac{K^{\text{eff}}}{I}} = \frac{ar\sin(2\bar{\theta})}{\bar{l}}\sqrt{\frac{k_e}{M}}. \quad \text{[S17]}$$

The sine-Gordon soliton solution in the spinner phase suggests an analogy with the well-known mechanical model consisting of a chain of pendula coupled via torsional springs (1). However, a side view of the model spinner chain in Fig. 7*B* suggests several important differences between the two models. First, unlike for the chain of coupled pendula, the springs connecting neighboring rods in our model have nonzero equilibrium projection in the plane of rotation of the rods and thus the even- and odd-numbered sites have different equilibrium positions. Second, the rotors do not all rotate about the same axis, but adjacent axes are displaced by the lattice spacing a in the x direction (Fig. 7). This breaks the global rotational symmetry of the chain. Moreover, as for the flipper phase, the sine-Gordon soliton has a nonzero topological charge originating from the term linear in θ'. This charge ensures that the static kink has zero energy, whereas in the dynamical case, it lowers the total energy of the soliton by a constant factor.

Linearized Perturbation Theory for the Wobbling Flipper

We now construct a simple model to qualitatively understand the wobbling flipper phase of motion as a superposition of the ϕ^4 flipper kink and linear perturbations around its asymptotic states. Because the wobbling flipper phase is observed for $d > 1$ (where $d = 2r\sin\bar{\theta}/a$), we find that to correctly account for the spatial period and decay length of the oscillations around the flipper kink, the linear theory must bear signatures of the spinner phase of motion (Eq. **4** and the subsequent discussion in the main text).

We show the main phenomena as we increase d in the wobbling flipper phase in Figs. S1 and S2. The static profile of the wobbling flipper is distinguished from that of the nonwobbling flipper by oscillations in u around the value $\bar{u}$. For small $d - 1$, the profile is indistinguishable by eye from the hyperbolic tangent profile of the nonwobbling flipper, as the amplitude of the oscillations is small, although subtracting off that profile as a background makes the deviation visible. As d increases, the amplitude increases; we found that the dependence of the maximum deviation above the equilibrium value $u = \bar{u}$ was proportional to d^3. Furthermore, the wavelength of the oscillations seems to stabilize at $2a$. The function $e^{-x/w_s}\cos(\pi x/a)$ was found to fit the oscillations for large enough x/a and d.

In the following, we approximate the oscillations observed in the wobbling phase (Fig. 5, *Upper Left Inset*) as small perturbations around the uniform ground state $\theta = \pm\bar{\theta}$ that the kink profiles approach asymptotically. Because the width of the flipper kink decreases inversely as $w \sim d^{-1}$, the asymptotic values are reached within a few lattice spacings for larger values of d.

We begin with Eq. **5** in the main text, the equation constraining two adjacent rotor angles θ_n, θ_{n+1}:

$$\cos(\theta_n + \theta_{n+1}) - \cos(2\bar{\theta}) + \frac{a}{r}(\sin\theta_n - \sin\theta_{n+1}) = 0. \quad \text{[S18]}$$

However, now we keep a few more terms in the continuum limit, again by taking a Taylor series around $x = n + \frac{1}{2}$:

$$\theta_n \to \theta\left(n - \frac{1}{2}\right) \approx \theta(x) - \frac{a}{2}\frac{d\theta}{dx} + \frac{a^2}{8}\frac{d^2\theta}{dx^2},$$
$$\theta_{n+1} \to \theta\left(n + \frac{1}{2}\right) \approx \theta(x) + \frac{a}{2}\frac{d\theta}{dx} + \frac{a^2}{8}\frac{d^2\theta}{dx^2}.$$

To this order, we obtain

$$\cos 2\left(\theta + \frac{a^2}{8}\frac{d^2\theta}{dx^2}\right) - \cos(2\bar{\theta}) + \frac{a^2}{r}\left(\frac{d(\sin\theta)}{dx}\right) = 0. \quad \text{[S19]}$$

Observe that this continuum limit respects the reflection symmetry $(x, \theta) \to (-x, -\theta)$.

It is convenient to define $\theta^* = \theta + (a^2/8)(d^2\theta/dx^2)$. Note that $\cos(2x) - \cos(2y) = (\sin x + \sin y)(\sin y - \sin x)$. We use this fact and then (after multiplying through by r^2) use the approximation $\sin\bar{\theta} + \sin\theta^* \approx 2\sin\bar{\theta}$ as we wish to consider the behavior when $\theta \approx \bar{\theta}$:

$$2r^2(2\sin\bar{\theta})(\sin\theta^* - \sin\bar{\theta}) + a^2 r\left(\frac{d(\sin\theta)}{dx}\right) = 0. \quad \text{[S20]}$$

We assume that $\epsilon = (a^2/8)(d^2\theta/dx^2)$ is small enough that $\sin\epsilon \approx \epsilon$ and $\cos\epsilon \approx 1$. Then

$$2r^2(2\sin\bar{\theta})\left(\sin\theta-\sin\bar{\theta}+\frac{a^2\cos\theta}{8}\frac{d^2\theta}{dx^2}\right)+a^2r\left(\frac{d(\sin\theta)}{dx}\right)=0. \quad \textbf{[S21]}$$

As usual, let $u = r\sin\theta$ and $\bar{u} = r\sin\bar{\theta}$. A consequence of our assumptions is that $d^2u/dx^2 \approx r^2\cos\theta(d^2\theta/dx^2)$ (neglecting a term nonlinear in u). Then

$$4\bar{u}\left(u-\bar{u}+\frac{a^2}{8}\frac{d^2u}{dx^2}\right)+a^2\frac{du}{dx}=0 \quad \textbf{[S22]}$$

$$\frac{a^2}{8}\frac{d^2(\delta u)}{dx^2}+\frac{a^2}{4\bar{u}}\frac{d(\delta u)}{dx}+\delta u=0. \quad \textbf{[S23]}$$

In the last line, we introduce $\delta u \equiv u-\bar{u}$. The solutions to Eq. **S23** are linear combinations of complex exponentials. In particular,

$$\delta u = Ae^{\lambda_- x}+Be^{\lambda_+ x}, \quad \textbf{[S24]}$$

where

$$\lambda_\pm = -\frac{1}{\bar{u}}\pm\sqrt{\frac{1}{\bar{u}^2}-\frac{8}{a^2}}. \quad \textbf{[S25]}$$

Provided $1/\bar{u} < \sqrt{8}/a$ or $d > 1/\sqrt{2}$, $\lambda_\pm$ are a complex conjugate pair, with real parts equal to $1/\bar{u}$ (as observed in Figs. S1 and S2) and imaginary parts approaching $\pm\sqrt{8}i/a \approx 2.8ia$ (compared with the wavenumber of $\pi i/a \approx 3.1i/a$ that we observe). Thus, for sufficiently large d, this linearized perturbation theory captures the fact that the decay length of the oscillations is equal to $\bar{u} = r\sin\bar{\theta}$, the width of the spinner soliton, and the wavenumber is on the order of the lattice spacing. In the opposite limit $(d < 1/\sqrt{2})$, both roots are real negative and thus the solution is simply an exponential decay, agreeing qualitatively with the shape of the tail of the hyperbolic tangent kink solution in the nonwobbling flipper phase.

We conjecture that with a more sophisticated expansion (e.g., with higher-order terms or some treatment of the nonlinear effects), the value of $\bar{u}/a$ and d at which we begin to see oscillations (and hence represents the transition between nonwobbling and wobbling flippers) should approach 1, and the imaginary part should approach $\pi i/a$.

1. Dauxois T, Peyrard M (2006) *Physics of Solitons* (Cambridge Univ Press, Cambridge, UK), pp 42–44.

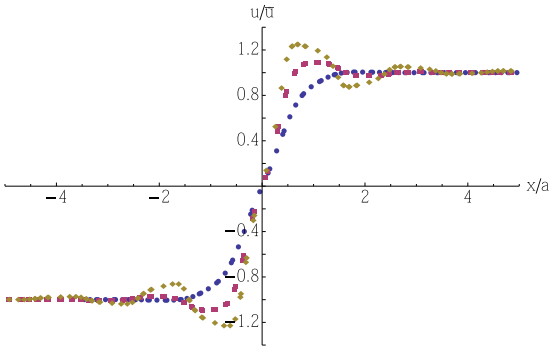

Fig. S1. The numerically generated displacement field $u(x - vt)$ (symbols) for various r/a in the wobbling flipper phase. These results are for a chain of 100 rods with $\bar{\theta} = 0.77$ and $k_e = 1$, $M = 1$; with $r/a = 0.8$, $d = 1.1$ (blue); with $r/a = 1.2$, $d = 1.7$ (magenta); and with $r/a = 1.6$, $d = 2.2$ (gold). The data arise from 10 snapshots of a single trajectory, translated so that the center of the soliton is at $x = 0$.

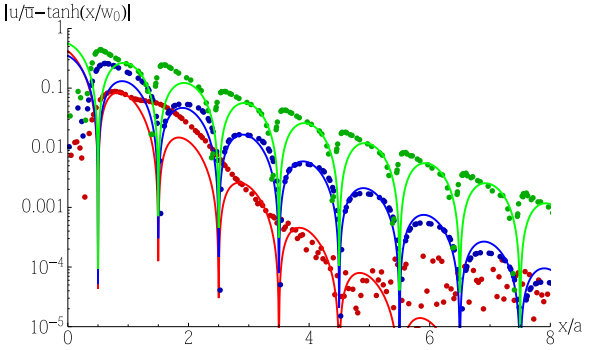

Fig. S2. The oscillations in numerically generated displacement fields $u(x - vt)$ (solid circles) in the wobbling flipper phase compared with the functions $e^{-x/w_s}\cos(\pi x/a)$ (solid lines). Oscillations are quantified by subtracting off the hyperbolic tangent flipper solution. The numerical results are for a chain of 100 rods with $\bar{\theta} = 0.77$ and $k_e = 1$, $M = 1$; with $r/a = 0.8$, $d = 1.1$ (red); with $r/a = 1.3$, $d = 1.8$ (blue); and with $r/a = 2.0$, $d = 2.8$ (green). The solid lines have a decay length of $w_s/a = (r/a)\sin\bar{\theta} = d/2$ with the same values of r/a, d. The data arise from 10 snapshots of a single trajectory, translated so that the center of the soliton is at $x = 0$.

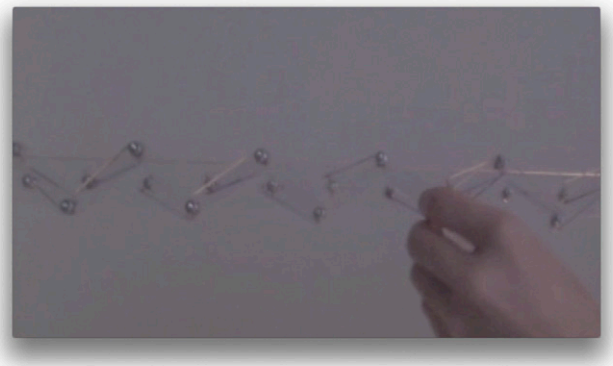

Movie S1. A model of the chain of rotors that is rigid in the bulk due to the acoustic modes being gapped and with an exponentially localized zero mode at the end. These illustrate predictions of the linear theory.

Movie S1

Movie S2. How the exponentially localized mode integrates into a moving domain wall in the model chain.

Movie S2

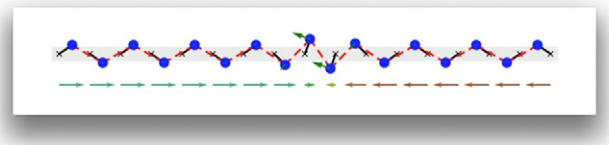

Movie S3. A simulation (Newtonian dynamics) of the full cycle of a (nonwobbling) flipper soliton in a chain of 17 rotors. The geometrical parameters of the chain are $a = 1$, $r = 0.5$, and $\overline{\theta} = 0.97$. The other model parameters are $k_e = 1{,}000$, $M = 1$, and $v_0 = 0.08$. The green arrows on each rotor are proportional to the angular velocity, and the red and blue arrows underneath depict the x projections of the rotors, showing the domain wall nature of the soliton.

Movie S3

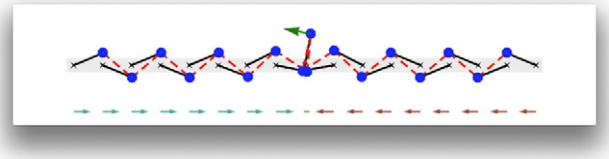

Movie S4. A simulation of the full cycle of a wobbling flipper soliton in a chain of 17 rotors. The geometrical parameters of the chain are $a = 1$, $r = 1.1$, and $\overline{\theta} = 1.18$. The other model parameters are $k_e = 1{,}000$, $M = 1$, and $v_0 = 0.04$. The green arrows on each rotor are proportional to the angular velocity, and the red and blue arrows underneath depict the x projections of the rotors, showing the domain wall nature of the soliton.

Movie S4

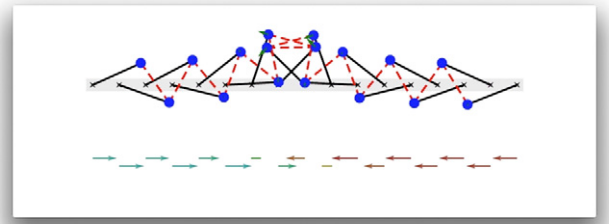

Movie S5. A simulation of the full cycle of a spinner soliton in a chain of 17 rotors. The geometrical parameters of the chain are $a = 1$, $r = 2$, and $\overline{\theta} = 1.18$. The other model parameters are $k_e = 1{,}000$, $M = 1$, and $v_0 = 0.04$. The green arrows on each rotor are proportional to the angular velocity, and the red and blue arrows underneath depict the x projections of the rotors, showing the domain wall nature of the soliton. We offset the x projections of the odd- and even-numbered sites to emphasize that the angles of odd rotors and even rotors converge separately to smooth functions differing by a constant.

Movie S5

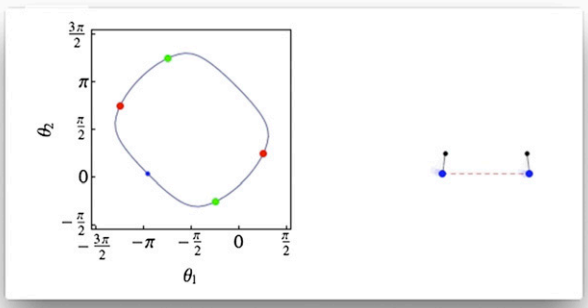

Movie S6. A unit cell of a chain in the (nonwobbling) flipper phase and its allowed motion in the configuration space spanned by the two rotor angles. The geometrical parameters of the chain are $a = 1$, $r = 0.25$, and $\overline{\theta} = 0.79$.

Movie S6

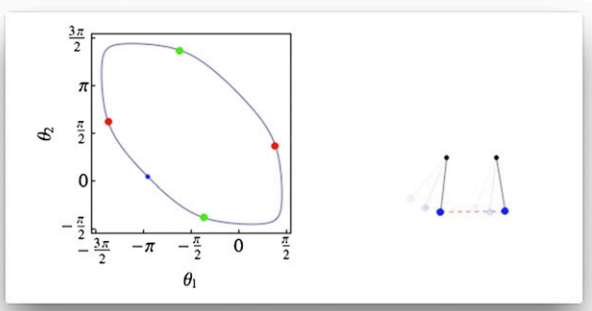

Movie S7. A unit cell of a chain in the wobbling flipper phase and its allowed motion in the configuration space spanned by the two rotor angles. The geometrical parameters of the chain are $a = 1$, $r = 1.1$, and $\bar{\theta} = 1.18$.

Movie S7

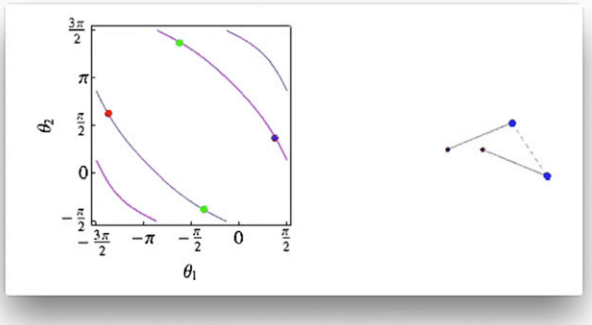

Movie S8. A unit cell of a chain in the spinner phase and its allowed motion in the configuration space spanned by the two rotor angles. The geometrical parameters of the chain are $a = 1$, $r = 2$, and $\bar{\theta} = 1.18$.

Movie S8

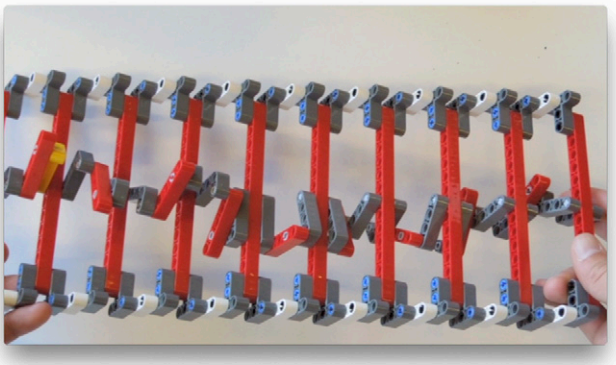

Movie S9. A model of the chain of rotors made out of LEGOs in the spinner phase.

Movie S9